Check for updates

Geophysical Research Letters

RESEARCH LETTER
10.1029/2026GL122108

Decoding Biases in Simulated Time-Mean Equatorial Pacific Subsurface Temperatures

Aoyun Xue[1], Xinyi Yuan[2,3], Wenjun Zhang[4], Fei-Fei Jin[5], Andrew T. Wittenberg[6], Xin Geng[4], and Chao Liu[7]

[1]Bren School of Environmental Science and Management, University of California, Santa Barbara, CA, USA, [2]Jiangsu Meteorological Service Center, Nanjing, China, [3]Key Laboratory of Transportation Meteorology, CMA, Nanjing, China, [4]CIC-FEMD/KLME, State Key Laboratory of Climate System Prediction and Risk Management, Nanjing University of Information Science and Technology, Nanjing, China, [5]Department of Atmospheric Sciences, SOEST, University of Hawai'i at Mānoa, Honolulu, HI, USA, [6]Geophysical Fluid Dynamics Laboratory, NOAA, Princeton, NJ, USA, [7]School of Earth and Environmental Sciences, Seoul National University, Seoul, Republic of Korea

Abstract Equatorial subsurface ocean temperature (*Tsub*) strongly influences tropical Pacific climate variability, yet the Coupled Model Intercomparison Project Phase 5 (CMIP5) and Phase 6 (CMIP6) models exhibit persistent *Tsub* cold biases and substantial inter-model uncertainty. Here we diagnose both systematic biases and inter-model spread in historical *Tsub* by applying a linear decomposition based on three key parameters: warm-pool temperature, thermocline depth, and thermocline sharpness. Cooler *Tsub* tends to occur in models with a cooler warm pool, shallower thermocline, and sharper stratification. These parameters explain most of the systematic biases and inter-model spread in *Tsub* among the CMIP historical simulations. Thermocline sharpness consistently dominates the systematic *Tsub* biases, whereas thermocline depth emerges as the primary source of inter-model spread in CMIP6. Our method provides an efficient empirical diagnosis of *Tsub* biases and model uncertainty that can help guide future model development.

Plain Language Summary Subsurface ocean long-term mean temperatures in the equatorial Pacific play a central role in regulating climate variability, such as the El Niño-Southern Oscillation. Yet many climate models struggle to realistically simulate these temperatures, and there remain substantial differences among models. Using statistical techniques, we find that most of these differences can be traced to three basic features of the tropical Pacific upper ocean: the surface temperature in the western Pacific warm pool region, the depth of the transition to cooler temperatures (the thermocline) at the base of the warm surface layer, and the abruptness of that transition. Models that simulate colder subsurface temperatures tend to exhibit a cooler warm pool, a shallower thermocline, and/or a sharper thermocline. While recent models have improved in some aspects, many still struggle to generate realistic thermocline depth and sharpness. By clarifying the sources of these model biases, our results can help to guide ongoing efforts to improve climate simulations.

Key Points:

- CMIP6 models exhibit significant subsurface temperature biases comparable to those in CMIP5, despite some differences in model behaviors
- These biases and model uncertainty are statistically linked to deviations in warm-pool sea surface temperature, thermocline depth, and thermocline sharpness
- Thermocline sharpness dominates systematic subsurface temperature biases, while thermocline depth controls CMIP6 inter-model spread

Supporting Information:

Supporting Information may be found in the online version of this article.

Correspondence to:

X. Yuan,
18252083636@163.com

Citation:

Xue, A., Yuan, X., Zhang, W., Jin, F.-F., Wittenberg, A. T., Geng, X., & Liu, C. (2026). Decoding biases in simulated time-mean equatorial Pacific subsurface temperatures. *Geophysical Research Letters*, *53*, e2026GL122108. https://doi.org/10.1029/2026GL122108

Received 30 JAN 2026
Accepted 19 MAR 2026

Author Contributions:

Conceptualization: Aoyun Xue, Xinyi Yuan, Fei-Fei Jin
Investigation: Aoyun Xue
Methodology: Aoyun Xue, Xinyi Yuan, Fei-Fei Jin, Andrew T. Wittenberg
Software: Aoyun Xue
Supervision: Xinyi Yuan, Wenjun Zhang
Visualization: Aoyun Xue
Writing – original draft: Aoyun Xue
Writing – review & editing: Xinyi Yuan, Wenjun Zhang, Andrew T. Wittenberg, Xin Geng, Chao Liu

© 2026. The Author(s).
This is an open access article under the terms of the Creative Commons Attribution License, which permits use, distribution and reproduction in any medium, provided the original work is properly cited.

1. Introduction

Tropical Pacific temperature variability shapes the global climate across timescales, with the El Niño-Southern Oscillation (ENSO) exerting powerful worldwide impacts (e.g., Alexander et al., 2002; Beniche et al., 2024; Wallace et al., 1998; W. Zhang et al., 2016). ENSO's characteristics and impacts are in turn shaped by the tropical Pacific background time-mean state, which modulates coupled ocean-atmosphere interactions and feedbacks (Bjerknes, 1969; Cane & Zebiak, 1985; Jin, 1996; Philander, 1983).

Global coupled general circulation models (CGCMs) are valuable tools for simulating and predicting the basic features and climate impacts of ENSO (e.g., Bellenger et al., 2014; Latif et al., 2001). While substantial progress has been made in CGCM development, systematic biases in the time-mean state remain pervasive across multiple generations of the Coupled Model Intercomparison Project (CMIP), hindering their reliability for climate projections (e.g., Guilyardi et al., 2009; Mechoso et al., 1995; C. Wang et al., 2014). One of the most prominent and long-standing model biases is an overly intense and meridionally-narrow equatorial Pacific sea surface temperature (SST) cold tongue that extends too far west, accompanied by excessive surface easterly trade winds and westward currents (e.g., Hwang & Frierson, 2013; Li & Xie, 2014; Wittenberg et al., 2006), which degrades ENSO simulation and contributes to uncertainty in future projections (e.g., Bayr et al., 2018; Guilyardi, 2006; Luo

19448007, 2026, 7, Downloaded from https://agupubs.onlinelibrary.wiley.com/doi/10.1029/2026GL122108 by CochraneChina, Wiley Online Library on [08/11/2026]. See the Terms and Conditions (https://onlinelibrary.wiley.com/terms-and-conditions) on Wiley Online Library for rules of use; OA articles are governed by the applicable Creative Commons License

et al., 2017; McPhaden et al., 2011; Samanta et al., 2019; Sun et al., 2009; B. Wang & An, 2002; Zhou & Xie, 2015).

The equatorial Pacific cold tongue is maintained by a strong connection between surface and subsurface processes, primarily through cold water upwelling from the subsurface layer (Li & Xie, 2012; Ying et al., 2019). On multi-year time scales, the equatorial subsurface temperature (*Tsub*) is largely controlled by large-scale winds, in particular the zonal wind stress and wind stress curl near the equator. The zonal slope and zonal-mean depth of the equatorial thermocline are governed by the equatorial Sverdrup balance and associated recharge-discharge pathways (Jin, 1997; Sverdrup, 1947; Wyrtki, 1981), and by the intensity of the tropical overturning cells (Johnson et al., 2001; McCreary & Lu, 1994; Schott et al., 2004). Oceanic adjustments to changing wind forcings are rapidly communicated by equatorial Kelvin and off-equatorial Rossby waves, and the resulting changes in thermocline depth and stratification directly modulate the equatorial *Tsub*. Misrepresented *Tsub* structures in most climate models have a significant impact on the simulated cold tongue bias (Zheng et al., 2012).

Previous work has shown that the equatorial cold tongue bias can be amplified by overly strong dynamical cooling linked to subsurface errors (Li et al., 2015). *Tsub* biases may arise from deficiencies in vertical mixing parameterizations and vertical resolution (which can influence thermocline depth and sharpness), as well as from biases in the strength and vertical structure of the equatorial undercurrent (Canuto et al., 2004; Reichl et al., 2024; Wilson, 2000). In addition, biases in the amplitudes and patterns of off-equatorial winds can also alter the subsurface water that feeds into the equatorial Pacific (Wittenberg et al., 2018), further shaping the mean subsurface thermal structure. Beyond local equatorial dynamics, the subsurface biases near the equator may be influenced by remote signals from the South Pacific through subtropical–tropical exchange pathways (Q. Zhang et al., 2023). Despite the critical role of the subsurface ocean, systematic *Tsub* biases in CGCMs remain relatively underexplored. An in-depth understanding of *Tsub* biases is crucial for reducing ENSO simulation uncertainty in climate models.

This study aims to better characterize the drivers of the climatological *Tsub* biases in the CMIP5 and CMIP6 multi-model historical simulations, using a well-established three-dimensional analytical expression for *Tsub* (Yuan et al., 2020). We apply the analytical framework to the full three-dimensional *Tsub* field at each longitude–latitude grid point and model depth level. For clarity, in Sections 3–5 we summarize the main results using a representative metric *Te*, defined as *Tsub* averaged over 50–75 m, a depth range that exerts particularly strong control on SST variability.

2. Data and Methodology

2.1. Reanalysis and Model Data Sets

We utilize observational reanalysis estimates of monthly-mean oceanic temperatures from version 3.3.1 of the Simple Ocean Data Assimilation (SODA 3.3.1; Carton et al., 2018), and historical simulations from 24 CMIP5 (Taylor et al., 2012) and 36 CMIP6 (Eyring et al., 2016) models (Tables S1 and S2 in Supporting Information S1). We evaluate the CMIP simulations during the 1980–2015 period spanned by the SODA reanalysis, and all data sets are tri-linearly interpolated at a 10 m vertical interval and a horizontal resolution of 1° prior to comparison.

2.2. Methodology

2.2.1. Analytical Expression of *Tsub*

Tsub in the equatorial Pacific exhibits a sharp vertical transition across the thermocline. Building on the thermocline profile used in the Cane–Zebiak model (Zebiak & Cane, 1987) and its subsequent refinements (Jin, 1996), this structure is well represented by an analytical hyperbolic-tangent fit that captures the observed thermocline shape. *Tsub* is formulated as a three-dimensional field over the equatorial Pacific using a function with three physically interpretable and measurable parameters: the thermocline depth (h), the thermocline sharpness (h^*), and an upper reference temperature (T_r) (Yuan et al., 2020). The three-dimensional *Tsub* is expressed as:

$$Tsub(x,y,z) = T_r - (T_r - 20)\left(1 - \tanh\frac{h(x,y) - z}{h^*(x,y)}\right). \quad (1)$$

19448007, 2026, 7, Downloaded from https://agupubs.onlinelibrary.wiley.com/doi/10.1029/2026GL122108 by CochraneChina, Wiley Online Library on [08/11/2026]. See the Terms and Conditions (https://onlinelibrary.wiley.com/terms-and-conditions) on Wiley Online Library for rules of use; OA articles are governed by the applicable Creative Commons License

Here, h denotes the local depth of the 20°C isotherm, h^* characterizes the local sharpness of thermocline, and T_r represents the warm-pool SST that serves as the upper bound of *Tsub*. The parameter h^* is inversely proportional to the density of subsurface isotherms:

$$h^*(x,y) = -(T_r - 20)/\left.\frac{\partial Tsub(x,y,z)}{\partial z}\right|_{z=h}. \quad (2)$$

Given longitude/latitude maps of h, h^*, and T_r, this analytical formulation can capture most of the observed equatorial *Tsub* structure across multiple reanalysis products down to about 300 m (Figure S1 in Supporting Information S1), below which the function asymptotically approaches its lower bound of 10°C. Although simplified, it represents the subsurface structure with three physically interpretable parameters that summarize the dominant controls on the *Tsub*. Specifically, large-scale winds and circulation control h through Sverdrup dynamics and the equatorial thermocline tilt (Li & Xie, 2012; Ying et al., 2019); equatorial upwelling, zonal currents and net surface heat flux modulate both h and T_r (Li et al., 2015); and vertical mixing, mesoscale/submesoscale eddies, diurnal-to-interannual thermocline depth fluctuations and bio-optical effects regulate h^* (e.g., Moum et al., 2009, 2013; Murtugudde et al., 2002; Ogata et al., 2013; Vannière et al., 2013; Whitt et al., 2022). In this way, the framework compactly integrates the net influence of these diverse processes and provides a physically interpretable basis for diagnosing *Tsub* biases. Further details on the *Tsub* expression can be found in Yuan et al. (2020).

Considering the excessively westward extension of the cold tongue in most CMIP models, we define the warm-pool SST (T_r) in each model in the following steps: First, we select a fixed box in the tropical western Pacific (15°S–15°N, 140°–170°E). Within the box, the warm pool is defined as the subset of grid points whose climatological SST exceeds the box-mean SST (Figures S2 and S3 in Supporting Information S1). We then compute T_r as the area-averaged SST over this warm pool subset. This method effectively reduces the influence of cold SSTs in the warm pool definition.

2.2.2. Linear Attribution of Biases and Inter-Model Differences in *Tsub*

Based on the three-dimensional *Tsub* statistical expression (Equation 1), the multi-model ensemble (MME) mean climatological *Tsub* is expressed as:

$$T_{subm} = T_{rm} - (T_{rm} - 20)\left(1 - \tanh\frac{h_m - z}{h_m^*}\right), \quad (3)$$

where the subscript "m" denotes the MME mean of each variable. Similarly, the climatological *Tsub* for an individual model j is given by:

$$T_{subj} = T_{rj} - (T_{rj} - 20)\left(1 - \tanh\frac{h_j - z}{h_j^*}\right). \quad (4)$$

The inter-model differences of *Tsub* are defined as the deviation of each model from the MME mean. Subtracting Equation 3 from Equation 4 gives the inter-model *Tsub* difference:

$$\Delta T_{subj} = \Delta T_{rj}\tanh\frac{h_m - z}{h_m^*} + (T_{rm} + \Delta T_{rj} - 20)\left(\tanh\frac{h_j - z}{h_j^*} - \tanh\frac{h_m - z}{h_m^*}\right). \quad (5)$$

ΔT_{rj} represents the inter-model difference between T_{rj} and T_{rm}. We then linearize Equation 5 using a first-order Taylor expansion to simplify the ΔT_{subj} expression:

$$\Delta T_{subj} = \Delta T_{rj}\tanh\left(\frac{h_m - z}{h_m^*}\right) + (T_{rm} - 20)\left[\cosh\left(\frac{h_m - z}{h_m^*}\right)\right]^{-2}\left(\frac{\Delta h_j}{h_m^*} - \frac{h_m - z}{h_m^*}\frac{\Delta h_j^*}{h_m^*}\right), \quad (6)$$

19448007, 2026, 7, Downloaded from https://agupubs.onlinelibrary.wiley.com/doi/10.1029/2026GL122108 by CochraneChina, Wiley Online Library on [08/11/2026]. See the Terms and Conditions (https://onlinelibrary.wiley.com/terms-and-conditions) on Wiley Online Library for rules of use; OA articles are governed by the applicable Creative Commons License

Δh_j and Δh_j^* represent the inter-model differences of h and h*, respectively. To simplify the notation, we define $\overline{H} = \frac{h_m - z}{h_m^*}$ as the baseline ratio of the MME mean h_m to h_m^* and introduce three coefficients:

$$F_{Tr} = \tanh(\overline{H}),$$

$$F_h = (T_{rm} - 20)\left[\cosh(\overline{H})\right]^{-2}\frac{1}{h_m^*}, \tag{7}$$

$$F_{h^*} = -\overline{H}F_h.$$

Equation 6 is rewritten as follows:

$$\Delta T_{subj} = F_{Tr}\Delta T_{rj} + F_h\Delta h_j + F_{h^*}\Delta h_j^*. \tag{8}$$

The coefficients F_{Tr}, F_h, and F_{h^*} are obtained directly from the MME mean state. Physically, F_{Tr} measures how warm-pool SST differences project onto *Tsub*, such that a positive T_r difference acts to warm subsurface water. F_h quantifies the sensitivity of *Tsub* to h differences, linking a biased vertical displacement of the thermocline to temperature changes at a given subsurface level. F_{h^*} captures the influence of h* difference, indicating how differences in thermocline sharpness and the associated vertical stratification modulate *Tsub*. The full derivation can be found in Text S1 in Supporting Information S1.

To quantify how these three factors shape the dominant pattern of inter-model *Tsub* variability, we perform an inter-model EOF analysis of *Te* differences (averaged over 50–75 m) across models (e.g., Ham & Kug, 2015; Hu et al., 2020; Li & Xie, 2012), defined as each model's *Te* departure from the MME mean, which serves as a compact metric of upper-thermocline *Tsub*. We focus on the leading mode (EOF1) of inter-model *Te* differences, which dominantly captures the total variance (>90%). We then project the linear decomposition (Equation 8) onto this mode and express the corresponding principal component (PC1) as a linear combination of inter-model T_r differences (ΔT_{rj}) and the leading-mode amplitudes of h and h* (i.e., $\mathrm{PC1}_h$ and $\mathrm{PC1}_{h^*}$):

$$\mathrm{PC1}_j \approx a\Delta T_{rj} + b\mathrm{PC1}_{hj} + c\mathrm{PC1}_{h^*j}, \tag{9}$$

where a, b and c are constant, model-independent coefficients that quantify the relative contributions of three factors to the leading PC1 of inter-model *Te*. This framework enables model-by-model attribution of factor contributions to inter-model *Te* differences, and, at the ensemble level, partitions the associated inter-model spread within CMIP5 and CMIP6 (Text S2 in Supporting Information S1). Specifically, multiplying Equation 9 by $\mathrm{PC1}_j$ and summing over all models yields:

$$\sum_j \mathrm{PC1}_j^2 = a\sum_j(\Delta T_{rj}\times\mathrm{PC1}_j) + b\sum_j(\mathrm{PC1}_{hj}\times\mathrm{PC1}_j) + c\sum_j(\mathrm{PC1}_{h^*j}\times\mathrm{PC1}_j). \tag{10}$$

which provides a variance-based partitioning of the EOF1 spread into contributions from three factors. By replacing the MME mean state with the observed state, this linear framework also attributes the MME mean bias relative to observations into contributions to the three factors (Text S3 in Supporting Information S1).

3. Biases and Inter-Model Spread of Climatological *Tsub* in the Equatorial Pacific

Consistent with previous studies (e.g., Bellenger et al., 2014; Li et al., 2015), the cold tongue bias persists in both model generations, with the simulated cold tongue extending westward by about 15–20° longitude in the MME compared to the observations (Figures S4a and S4b in Supporting Information S1). The SST bias is also zonally coherent and robust across models, with a comparatively modest inter-model spread (Figures S4c–S4f in Supporting Information S1).

This bias is not confined to the surface but also extends into the subsurface, influencing the entire thermal structure of the equatorial Pacific. Figure 1 shows the time-mean *Tsub* in the observations and in the MME means of CMIP5 and CMIP6. Both model generations exhibit systematic subsurface cold biases in the upper thermocline (Figures 1a and 1b). Additionally, the sparse distribution of isotherms above 20°C reveals that the subsurface

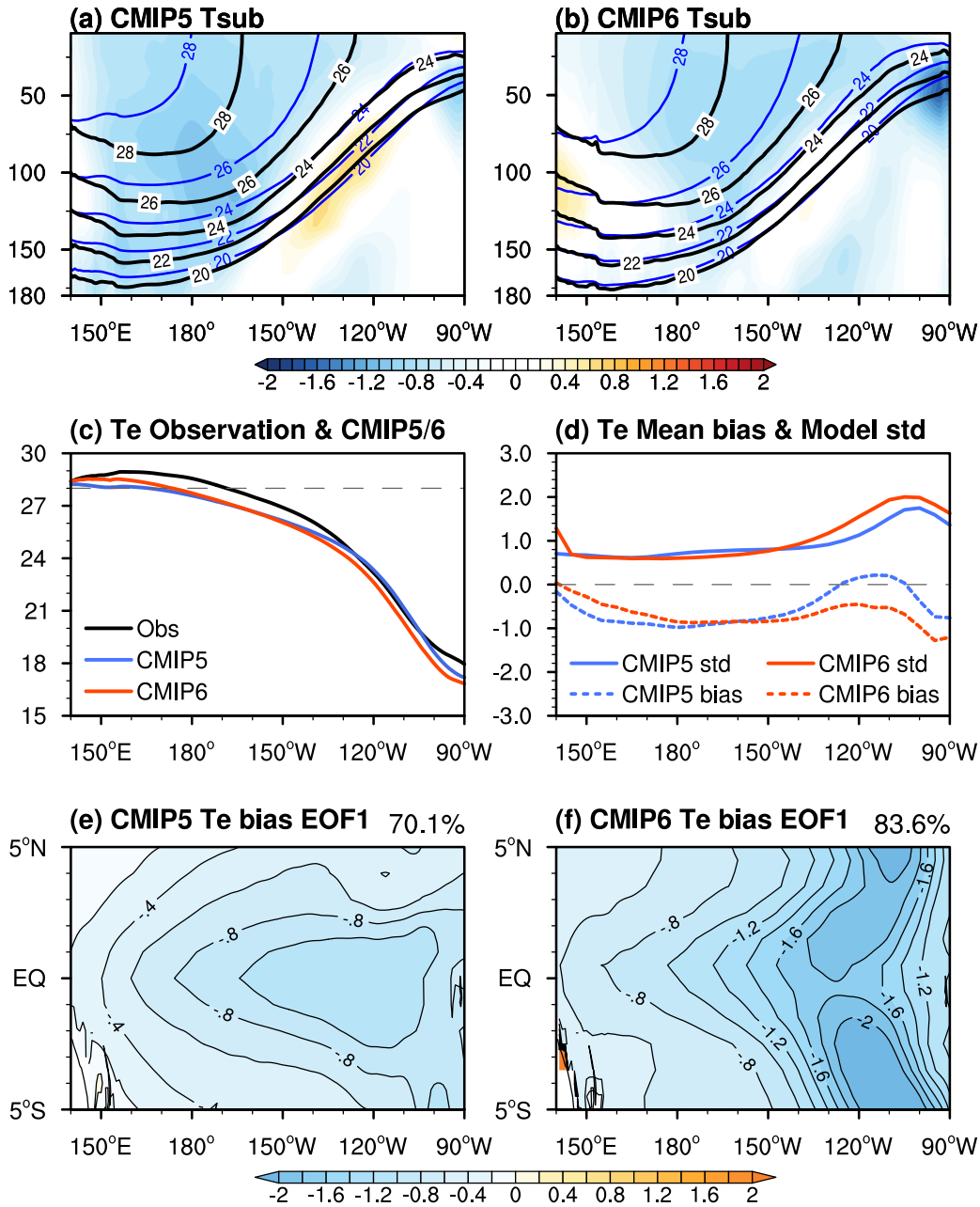


Figure 1. (a, b) *Tsub* biases (5°S–5°N average) relative to observations in CMIP5 and CMIP6 models (shadings), with black (blue) contours representing the observations (MME mean). (c) 5°S–5°N averaged *Te* (50–75 m) in observations (black), CMIP5 (blue) and CMIP6 (red). (d) As in (c), but for MME mean biases relative to observations (dashed lines) and inter-model standard deviation (solid lines) of *Te* for CMIP5 and CMIP6. (e, f) Leading EOF mode (EOF1) of inter-model *Te* differences for CMIP5 and CMIP6, with the percentage of explained variance indicated in the top-right corner of each panel.

stratification in the MME is weaker than observed, indicating that CMIP5 and CMIP6 models misrepresent equatorial thermocline sharpness (Tang et al., 2024).

Since subsurface temperature at 50–75 m in the equatorial Pacific has the most direct impact on SST variations (Yuan et al., 2020), we characterize subsurface biases using *Te* (50–75 m average). The results show that the MME mean *Te* is systematically colder than observed, with the largest cold biases in the central–western Pacific (CWP) for CMIP5 and in the eastern equatorial Pacific (EEP) for CMIP6 (Figures 1c and 1d). The standard

19448007, 2026, 7, Downloaded from https://agupubs.onlinelibrary.wiley.com/doi/10.1029/2026GL122108 by CochraneChina, Wiley Online Library on [08/11/2026]. See the Terms and Conditions (https://onlinelibrary.wiley.com/terms-and-conditions) on Wiley Online Library for rules of use; OA articles are governed by the applicable Creative Commons License

19448007, 2026, 7, Downloaded from https://agupubs.onlinelibrary.wiley.com/doi/10.1029/2026GL122108 by CochraneChina, Wiley Online Library on [08/11/2026]. See the Terms and Conditions (https://onlinelibrary.wiley.com/terms-and-conditions) on Wiley Online Library for rules of use; OA articles are governed by the applicable Creative Commons License

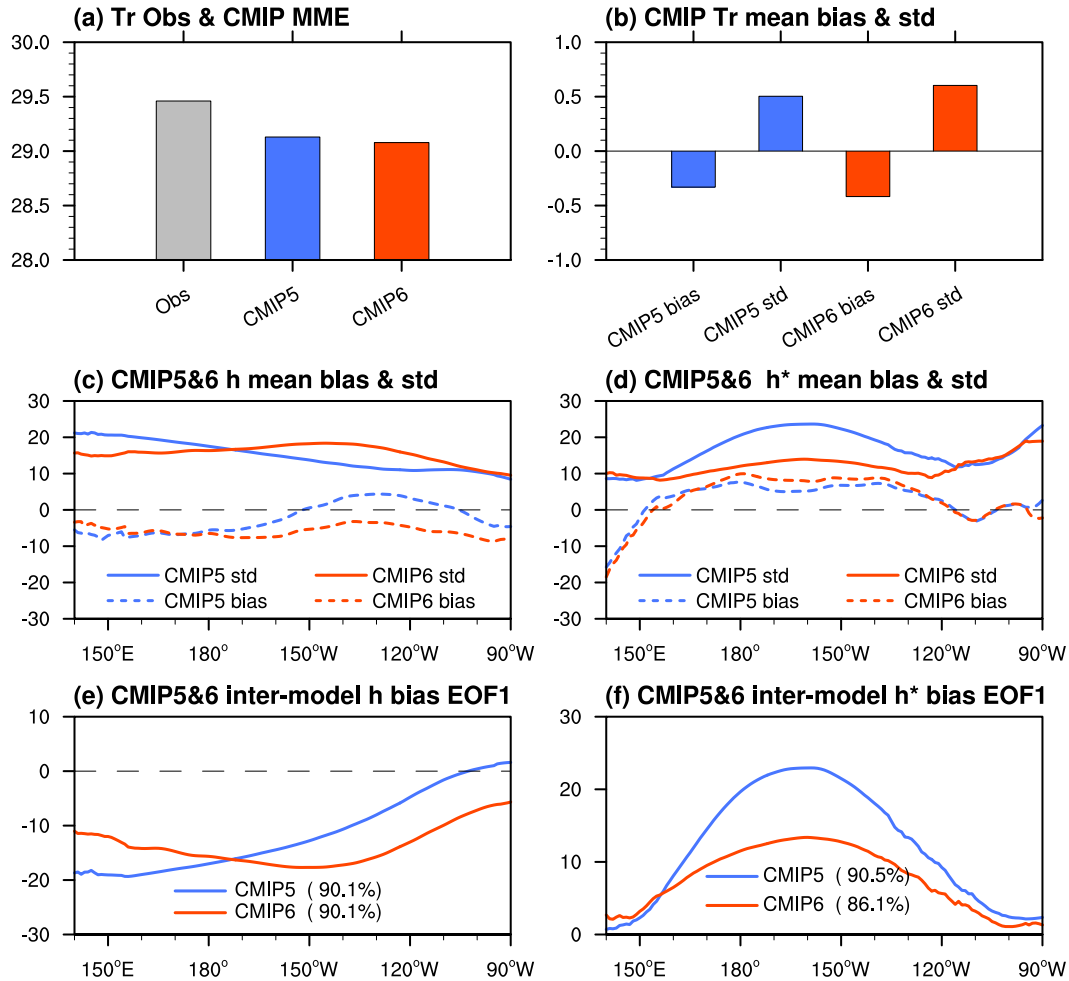


Figure 2. (a) Warm-pool sea surface temperature (T_r) from observations (gray) and the multi-model ensemble mean in CMIP5 (blue) and CMIP6 (red). (b) Ensemble-mean bias relative to observations and inter-model standard deviation of T_r. (c, d) Ensemble-mean biases relative to observations (dashed lines) and inter-model standard deviations (solid lines) for h and h^* averaged over 5°S–5°N in CMIP5 (blue) and CMIP6 (red), respectively. (e, f) Leading EOF patterns of inter-model differences of h and h^* (averaged over 5°S–5°N) in CMIP5 and CMIP6 models, shown as regression maps of the inter-model difference fields onto the corresponding standardized PC1.

deviation of inter-model *Te* differences is distributed across the equatorial Pacific but larger in the EEP for both ensembles (Figure 1d).

To further characterize the spatial structure of this spread, we compute EOFs of the inter-model *Te* differences (Figures 1e and 1f). EOF1 captures most of the total variance in both CMIP5 and CMIP6 (>70%) and is concentrated in the EEP, where thermocline dynamics and ENSO-related subsurface variations are most pronounced (Jin et al., 2006; Meinen & McPhaden, 2000; Vialard et al., 2025; Yeh et al., 2009). With PC1 normalized to unit variance, the larger values of EOF1 amplitude in CMIP6 indicate that model uncertainty in *Te* is more pronounced than in CMIP5. This result motivates a closer examination of the processes controlling both the mean biases and the inter-model spread in *Te*.

4. Biases and Inter-Model Spread in Three Key Factors Controlling *Tsub*

Based on the *Tsub* analytical formulation (Section 2.2.1), we examine the three key factors (i.e., T_r, h, h^*) that govern the systematic biases and inter-model *Te* differences in the CMIP models. Among these, T_r exhibits a modest cold bias in both generations: the observed T_r is approximately 29.5°C, while the MME means are ~29.1°C in CMIP5 and ~29.0°C in CMIP6 (Figure 2a). CMIP6 shows a slightly larger cold bias and larger inter-model

19448007, 2026, 7, Downloaded from https://agupubs.onlinelibrary.wiley.com/doi/10.1029/2026GL122108 by CochraneChina, Wiley Online Library on [08/11/2026]. See the Terms and Conditions (https://onlinelibrary.wiley.com/terms-and-conditions) on Wiley Online Library for rules of use; OA articles are governed by the applicable Creative Commons License

spread than CMIP5 (Figure 2b; Figures S5a and S5b in Supporting Information S1), indicating no systematic improvement and suggesting a possible degradation in T_r performance. The persistent bias and spread underscore that warm-pool SST remains a model deficiency that merits continued attention in model development.

We next assess the systematical biases and inter-model differences in thermocline depth h (averaged over 5°S–5°N). Compared to observations, both CMIP ensembles exhibit a shallower thermocline in the CWP, with CMIP6 extending this shoaling across most of the equatorial basin (Figure 2c). The inter-model spread is most pronounced in the central equatorial Pacific. The EOF1 of inter-model h differences explains ~90% of the variance in both ensembles, characterized by a basin-scale pattern centered in the central and eastern equatorial region (Figure 2e). While the corresponding PC1 further quantifies this diversity (Figures S5c and S5d in Supporting Information S1), the relationship between a shallower h and colder Te is not strictly proportional across models. This discrepancy suggests that Tr and h^* also play critical roles in shaping inter-model Te variability.

We further examine the model behavior of thermocline sharpness h^*. Both ensembles display a systematic bias, with the MME mean h^* approximately 6 m larger than the observation (Figure 2d), implying a more diffuse thermocline and weakened subsurface stratification. Although the inter-model spread peaks in the central equatorial Pacific, the amplitude of its leading EOF is smaller in CMIP6 than in CMIP5 (Figure 2f), reflecting a reduction in h^* diversity. The corresponding PC1 summarizes each model's departure along this dominant h^* pattern (Figures S5c and S5d in Supporting Information S1): models with higher PC1 (sharper thermoclines) tend to exhibit colder Te, consistent with enhanced near-surface vertical temperature gradient and greater sensitivity of subsurface temperatures to upwelling. Notably, the fact that significant inter-model Te differences can persist even under modest h variations underscores the independent and sometimes compensatory roles of h and h^* in shaping tropical Pacific climate simulations.

Overall, systematic biases and inter-model spread remains substantial across all three key factors, indicating persistent uncertainty in Te representation among CMIP models. Both the mean biases and inter-model standard deviation remain particularly large for h and h^* in the CWP and EEP. These results highlight the need for improving parameterizations of subgrid-scale eddy heat transport and vertical mixing in climate models to enhance their representation of equatorial Pacific climate dynamics.

5. Contributions of Three Factors to *Te* Biases and Inter-Model Spread

Using the inter-model EOF projection and the linear decomposition (Section 2.2.2), we quantify the contributions of three controlling factors (T_r, h, and h^*) to climatological Te biases and inter-model differences. Figures 3a–3d present the zonal structures of $\overline{H}$ (averaged over 5°S–5°N and 50–75 m) and the three coefficients (F_{Tr}, F_h and F_{h^*}) for observations and the CMIP MME mean. $\overline{H}$ decreases from west to east (Figure 3a), reflecting the climatological west-east thermocline tilt. The sensitivities exhibit distinct spatial structures (Figures 3b–3d): F_{Tr} is strongest over the CWP, F_h is largest and predominantly positive in the EEP, and F_{h^*} exhibits basin-wide structure with negative values over much of the CWP. Notably, the CMIP5 and CMIP6 MME means reproduce the observed zonal structures of $\overline{H}$ and the three coefficients, suggesting that large-scale sensitivity of Te to these factors is realistically represented across model generations.

The effectiveness of this linearized framework (Equation 9) is validated by the close agreement between the reconstructed and original inter-model Te differences. With PC1 correlations exceeding 0.9 for both ensembles (Figures 3e and 3f), the method effectively captures the primary drivers of systematic biases and inter-model Te variability. This fidelity is further supported by the consistent alignment of zonal profiles across the ensemble, confirming the robustness of our attribution (Figures S6 and S7 in Supporting Information S1).

We apply the decomposition framework to the ensemble-mean bias by treating the MME mean as a single "model" and observations as the reference (Figures 4a and 4b). This attribution quantifies how systematic biases in T_r, h, and h^* combine to produce the MME mean Te bias. The results show that thermocline structure remains central to the mean Te bias, with h^* contributing substantially in both CMIP5 and CMIP6 and additional contributions from T_r and h. This finding highlights the importance of improving the representation of thermocline sharpness and the associated vertical stratification in coupled climate models.

19448007, 2026, 7, Downloaded from https://agupubs.onlinelibrary.wiley.com/doi/10.1029/2026GL122108 by CochraneChina, Wiley Online Library on [08/11/2026]. See the Terms and Conditions (https://onlinelibrary.wiley.com/terms-and-conditions) on Wiley Online Library for rules of use; OA articles are governed by the applicable Creative Commons License

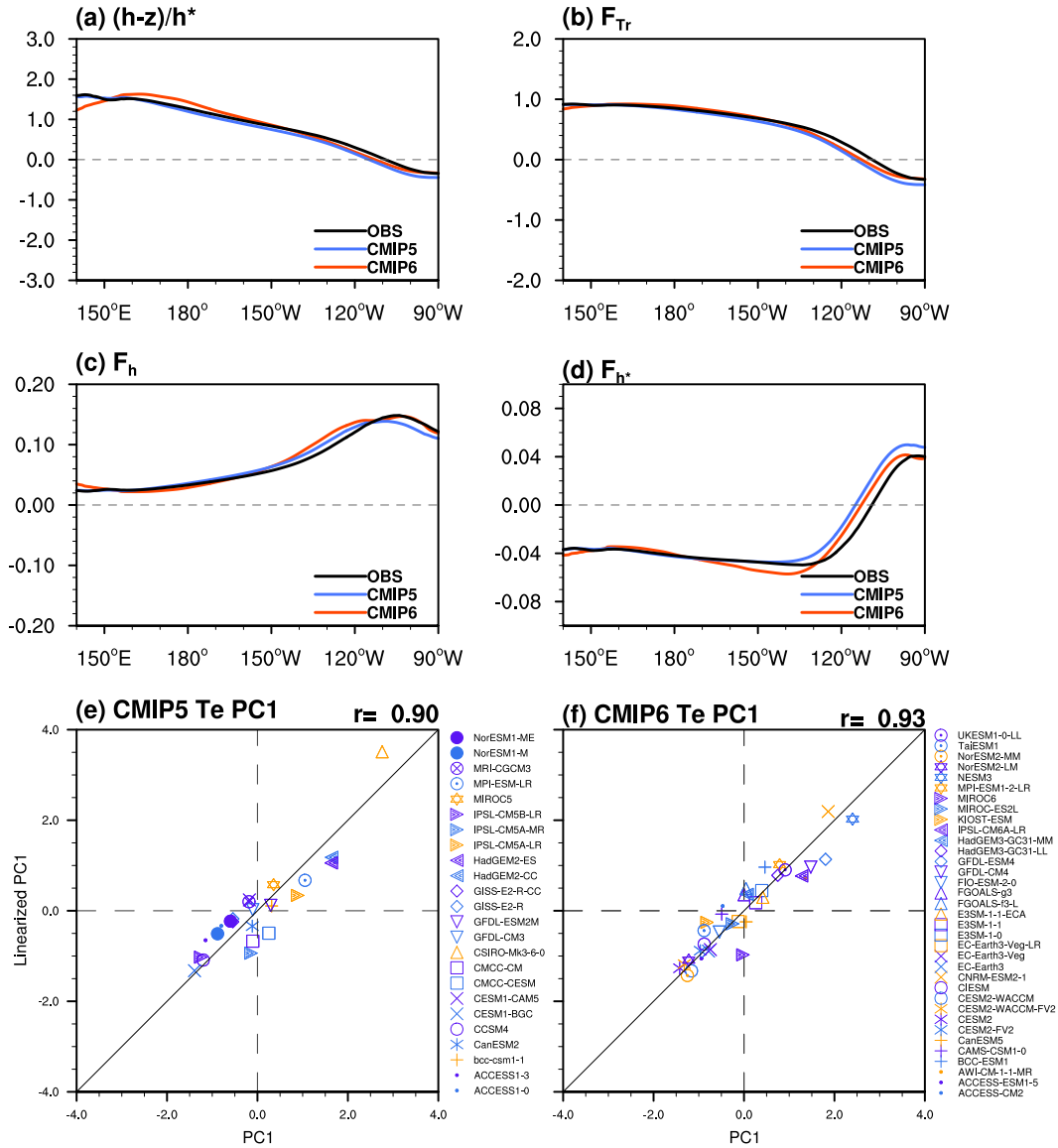


Figure 3. Zonal distributions of (a) the normalized thermocline depth term $\overline{H}$ (averaged over 5°S–5°N and 50–75 m), and the linear decomposition coefficient (b) F_{Tr}, (c) F_h, and (d) F_{h^*} for observations (black), CMIP5 (blue) and CMIP6 (red). For the observational curves, the coefficients are computed using observed T_r, h and h^*. F_{Tr}, F_h and F_{h^*} measure the sensitivity of Te to perturbations in warm pool reference temperature T_r, thermocline depth h, and thermocline sharpness h^*, respectively. (e, f) Relationship between the leading PC1 of the original and reconstructed inter-model Te differences for CMIP5 and CMIP6, with correlation coefficients of 0.90 and 0.93, respectively.

We further decompose the inter-model variance of Te into contributions from three key factors (Equation 10). The results show that CMIP5 inter-model spread is dominated by T_r and h^*, whereas in CMIP6 the contribution from h^* is reduced and h becomes the leading source of inter-model spread (Figures 4c and 4d). Notably, the h^* term in CMIP6 is slightly negative, indicating that h^* variations are out of phase with the leading mode and thus offset, rather than amplify, the inter-model variance. This shift indicates that CMIP6 has partially reduced uncertainties associated with h^*, but persistent errors in h remain a primary source of inter-model Te differences and a key target for further model development.

Using the linear decomposition (Section 2.2.2), we also quantify the relative contributions of T_r, h, and h^* to inter-model Te differences in individual models (Figure S8 in Supporting Information S1). Each factor can contribute with either sign, and the resulting Te differences reflect their combined effects. When these contributions

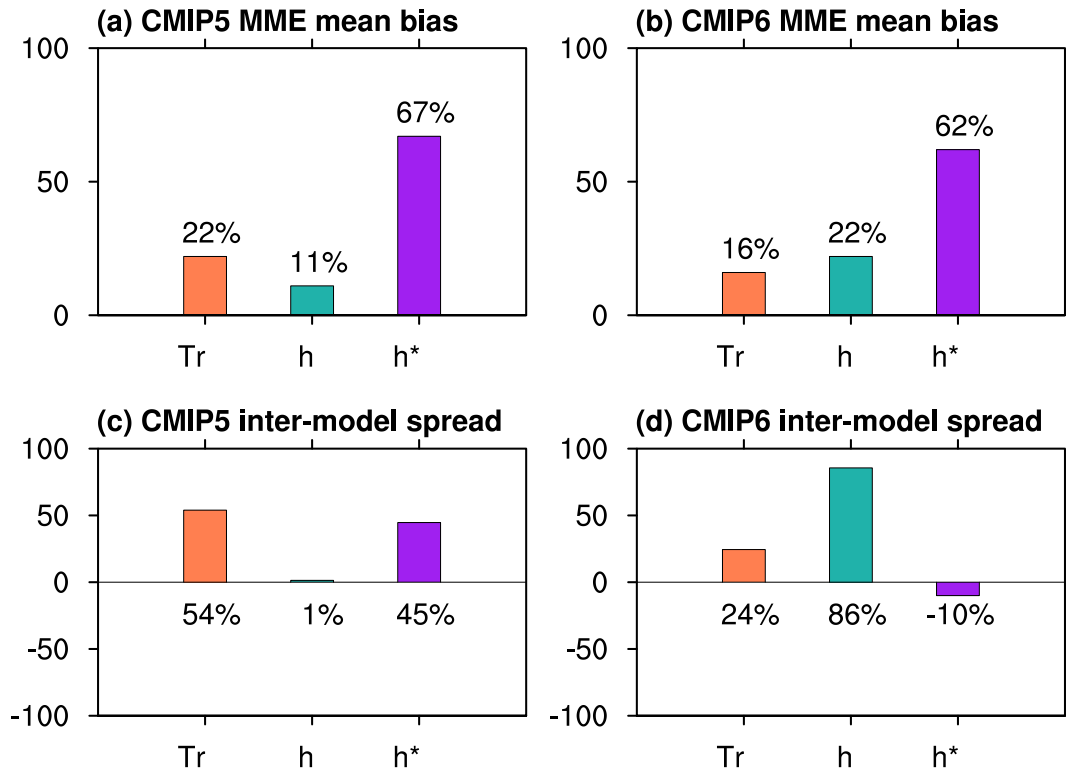


Figure 4. Relative contributions of warm-pool reference temperature (T_r; orange), thermocline depth (h; cyan), and thermocline sharpness (h*; purple), to (a, b) the MME mean *Te* bias relative to observations and (c, d) the inter-model *Te* spread over the equatorial Pacific (5°S–5°N, 140°E–90°W) for CMIP5 and CMIP6, respectively. Positive (negative) values indicate that the factor increases (reduces) the MME mean bias or inter-model spread.

compensate, *Te* stays close to the MME mean despite sizable deviations in individual factors; when they reinforce, large departures from the MME mean occur. Notably, substantial *Te* differences can also arise with only modest h contributions, indicating a dominant role for h* in some models. Together, these results show that reducing *Te* bias and inter-model uncertainty requires constraining both thermocline depth and sharpness, rather than relying on a single metric.

6. Conclusions and Discussion

This study diagnoses climatological *Tsub* biases and inter-model uncertainty in the equatorial Pacific across CMIP5 and CMIP6 historical simulations. Both ensembles exhibit a persistent cold *Tsub* bias relative to observations and substantial inter-model spread. In the MME mean, the cold bias is associated with a cooler SST (lower T_r), an overly shallow thermocline (smaller h), and an overly sharp, and/or an strongly stratified thermocline (smaller h*). Using a linear attribution framework derived from an established *Tsub* analytical expression, we find that the MME mean bias in both CMIP5 and CMIP6 is dominated by errors in thermocline sharpness h*, with smaller contributions from T_r and h. The variance decomposition further shows that CMIP5 spread is dominated by T_r and h*, whereas in CMIP6 the h* contribution is strongly reduced and h becomes the leading driver of the inter-model spread. At the individual model level, the three factors can offset or reinforce one another, so similar *Tsub* biases may arise from distinct combinations of T_r, h, and h* errors.

A key insight from this study is that thermocline depth alone cannot account for either the systematic bias or the inter-model uncertainty in *Tsub*. Instead, thermocline sharpness emerges as a crucial factor, exhibiting a strong association with *Tsub* structure in the equatorial Pacific. As thermocline structure plays a key role in regulating the mean state and ENSO variability, addressing subsurface thermocline biases, particularly in h and h*, can help reduce systematic SST and *Tsub* biases in coupled climate models.

19448007, 2026, 7, Downloaded from https://agupubs.onlinelibrary.wiley.com/doi/10.1029/2026GL122108 by CochraneChina, Wiley Online Library on [08/11/2026]. See the Terms and Conditions (https://onlinelibrary.wiley.com/terms-and-conditions) on Wiley Online Library for rules of use; OA articles are governed by the applicable Creative Commons License

19448007, 2026, 7, Downloaded from https://agupubs.onlinelibrary.wiley.com/doi/10.1029/2026GL122108 by CochraneChina, Wiley Online Library on [08/11/2026]. See the Terms and Conditions (https://onlinelibrary.wiley.com/terms-and-conditions) on Wiley Online Library for rules of use; OA articles are governed by the applicable Creative Commons License

While our analysis identifies T_r, h, and h^* as the dominant controls on *Tsub* biases, the underlying sources of these errors likely involve multiple coupled processes. For example, biases in surface wind stress and the resulting ocean circulation can distort equatorial upwelling and thermocline tilt, projecting primarily onto h. Biases in surface heat fluxes and cloud–radiative feedbacks can modify warm-pool temperature T_r (Ferrett et al., 2017, 2018), whereas limitations in vertical resolution and turbulent mixing parameterizations can influence the thermocline sharpness h^* and subsurface stratification. These pathways offer plausible origins for the diagnosed *Tsub* biases and motivate targeted process-oriented diagnostics and sensitivity experiments to isolate the dominant sources within specific model families. By providing a quantitative diagnosis of both systematic biases and inter-model uncertainty, this study offers a practical basis for improving simulations of the equatorial Pacific climate and future ENSO behavior.

Conflict of Interest

The authors declare no conflicts of interest relevant to this study.

Availability Statement

All data used in this study are publicly available. SODA3.3.1 data is available at https://apdrc.soest.hawaii.edu/dods/public_data/SODA/soda_3.3.1 (Carton et al., 2018). All CMIP5 and CMIP6 outputs are downloaded fromhttps://aims2.llnl.gov/search/cmip5/ (Taylor et al., 2012) and https://aims2.llnl.gov/search/cmip6/ (Eyring et al., 2016). The CMIP5 and CMIP6 models used in this study are listed in Tables S1 and S2 in Supporting Information S1. All analyses and figures were produced using NCAR Command Language (NCL) version 6.6.2 (The NCAR Command Language, 2019).

Acknowledgments
This work was supported by the National Natural Science Foundation of China (42205052). We wish to acknowledge the WCRP Working Group on Coupled Modeling, which is responsible for CMIP, and the climate modeling groups for producing and making available their model outputs.

References

Alexander, M. A., Blade, I., Newman, M., Lanzante, J. R., Lau, N. C., & Scott, J. D. (2002). The atmospheric bridge: The influence of ENSO teleconnections on air-sea interaction over the global oceans. *Journal of Climate*, *15*(6), 2205–2231. https://doi.org/10.1175/1520-0442(2002)015<2205:TABTIO>2.0.CO;2

Bayr, T., Latif, M., Dommenget, D., Wengel, C., Harlaß, J., & Park, W. (2018). Mean-state dependence of ENSO atmospheric feedbacks in climate models. *Climate Dynamics*, *50*(9–10), 3171–3194. https://doi.org/10.1007/s00382-017-3799-2

Bellenger, H., Guilyardi, E., Leloup, J., Lengaigne, M., & Vialard, J. (2014). ENSO representation in climate models: From CMIP3 to CMIP5. *Climate Dynamics*, *42*(7–8), 1999–2018. https://doi.org/10.1007/s00382-013-1783-z

Beniche, M., Vialard, J., Lengaigne, M., Voldoire, A., Srini, G., & Hall, N. M. J. (2024). A distinct and reproducible teleconnection pattern over North America during extreme El Niño events. *Scientific Reports*, *14*(1), 2457. https://doi.org/10.1038/s41598-024-52580-9

Bjerknes, J. (1969). Atmospheric teleconnections from the equatorial Pacific. *Monthly Weather Review*, *97*(3), 163–172. https://doi.org/10.1175/1520-0493(1969)097,0163:ATFTEP.2.3.CO;2

Cane, M. A., & Zebiak, S. E. (1985). A theory for El Niño and the Southern Oscillation. *Science*, *228*(4703), 1085–1087. https://doi.org/10.1126/science.228.4703.1085

Canuto, V. M., Howard, A., Cheng, Y., & Miller, R. L. (2004). Latitude-dependent vertical mixing and the tropical thermocline in a global OGCM. *Geophysical Research Letters*, *31*(16), L16305. https://doi.org/10.1029/2004GL019891

Carton, J. A., Chepurin, G. A., & Chen, L. (2018). SODA3: A new ocean climate reanalysis. *Journal of Climate*, *31*(17), 6967–6983. https://doi.org/10.1175/JCLI-D-18-0149.1

Eyring, V., Bony, S., Meehl, G. A., Senior, C. A., Stevens, B., Stouffer, R. J., & Taylor, K. E. (2016). Overview of the Coupled Model Intercomparison Project Phase 6 (CMIP6) experimental design and organization. *Geoscientific Model Development*, *9*(5), 1937–1958. https://doi.org/10.5194/gmd-9-1937-2016

Ferrett, S., Collins, M., & Ren, H. (2017). Understanding bias in the evaporative damping of El Niño–Southern Oscillation events in CMIP5 models. *Journal of Climate*, *30*(16), 6351–6370. https://doi.org/10.1175/JCLI-D-16-0748.1

Ferrett, S., Collins, M., & Ren, H. (2018). Diagnosing relationships between mean state biases and El Niño shortwave feedback in CMIP5 models. *Journal of Climate*, *31*(4), 1315–1335. https://doi.org/10.1175/JCLI-D-17-0331.1

Guilyardi, E. (2006). El Niño-mean state-seasonal cycle interactions in a multi-model ensemble. *Climate Dynamics*, *26*(4), 329–348. https://doi.org/10.1007/s00382-005-0084-6

Guilyardi, E., Wittenberg, A., Fedorov, A., Collins, M., Wang, C. Z., Capotondi, A., et al. (2009). Understanding El Niño in ocean-atmosphere general circulation models: Progress and challenges. *Bulletin of the American Meteorological Society*, *90*(3), 325–340. https://doi.org/10.1175/2008BAMS2387.1

Ham, Y.-G., & Kug, J.-S. (2015). Improvement of ENSO simulation based on intermodel diversity. *Journal of Climate*, *28*(3), 998–1015. https://doi.org/10.1175/JCLI-D-14-00376.1

Hu, X., Fan, H., Cai, M., Sejas, S. A., Taylor, P., & Yang, S. (2020). A less cloudy picture of the inter-model spread in future global warming projections. *Nature Communications*, *11*(1), 4472. https://doi.org/10.1038/s41467-020-18227-9

Hwang, Y.-T., & Frierson, D. M. M. (2013). Link between the double-Intertropical Convergence Zone problem and cloud biases over the Southern Ocean. *Proceedings of the National Academy of Sciences, USA*, *110*(13), 4935–4940. https://doi.org/10.1073/pnas.1213302110

Jin, F.-F., Kim, S. T., & Bejarano, L. (2006). A coupled-stability index for ENSO. *Geophysical Research Letters*, *33*(23), 2006GL027221. https://doi.org/10.1029/2006GL027221

Jin, F.-F. (1996). Tropical ocean-atmosphere interaction, the Pacific cold tongue, and the El Niño Southern Oscillation. *Science*, *274*(5284), 76–78. https://doi.org/10.1126/science.274.5284.76

Jin, F.-F. (1997). An equatorial ocean recharge paradigm for ENSO. Part I: Conceptual model. *Journal of the Atmospheric Sciences*, *54*(7), 811–829. https://doi.org/10.1175/1520-0469(1997)054<0811:aeorpf>2.0.co;2

Johnson, G. C., McPhaden, M. J., & Firing, E. (2001). Equatorial Pacific Ocean horizontal velocity, divergence, and upwelling. *Journal of Physical Oceanography*, *31*(3), 839–849. https://doi.org/10.1175/1520-0485(2001)031<0839:EPOHVD>2.0.CO;2

Latif, M., Sperber, K., Arblaster, J., Braconnot, P., Chen, D., Colman, A., et al. (2001). ENSIP: The El Niño simulation intercomparison project. *Climate Dynamics*, *18*(3-4), 255–276. https://doi.org/10.1007/s003820100174

Li, G., Du, Y., Xu, H., & Ren, B. (2015). An intermodel approach to identify the source of excessive equatorial Pacific cold tongue in CMIP5 models and uncertainty in observational datasets. *Journal of Climate*, *28*(19), 7630–7640. https://doi.org/10.1175/jcli-d-15-0168.1

Li, G., & Xie, S.-P. (2012). Origins of tropical-wide SST biases in CMIP multi-model ensembles. *Geophysical Research Letters*, *39*(22), L22703. https://doi.org/10.1029/2012GL053777

Li, G., & Xie, S.-P. (2014). Tropical biases in CMIP5 multimodel ensemble: The excessive equatorial Pacific cold tongue and double ITCZ problems. *Journal of Climate*, *27*(4), 1765–1780. https://doi.org/10.1175/JCLI-D-13-00337.1

Luo, J.-J., Wang, G., & Dommenget, D. (2017). May common model biases reduce CMIP5's ability to simulate the recent Pacific La Niña-like cooling? *Climate Dynamics*, *50*(3–4), 1335–1351. https://doi.org/10.1007/s00382-017-3688-8

McCreary, J. P., & Lu, P. (1994). Interaction between the subtropical and equatorial ocean circulations: The subtropical cell. *Journal of Physical Oceanography*, *24*(2), 466–497. https://doi.org/10.1175/1520-0485(1994)024<0466:IBTSAE>2.0.CO;2

McPhaden, M. J., Lee, T., & McClurg, D. (2011). El Niño and its relationship to changing background conditions in the tropical Pacific Ocean. *Geophysical Research Letters*, *38*(15), L15709. https://doi.org/10.1029/2011GL048275

Mechoso, C. R., Robertson, A. W., Barth, N., Davey, M. K., Delecluse, P., Gent, P. R., et al. (1995). The seasonal cycle over the tropical Pacific in coupled ocean–atmosphere general circulation models. *Monthly Weather Review*, *123*(9), 2825–2838. https://doi.org/10.1175/1520-0493(1995)123<2825:tscott>2.0.co;2

Meinen, C. S., & McPhaden, M. J. (2000). Observations of warm water volume changes in the equatorial Pacific and their relationship to El Niño and La Niña. *Journal of Climate*, *13*(20), 3551–3559. https://doi.org/10.1175/1520-0442(2000)013<3551:OOWWVC>2.0.CO;2

Moum, J. N., Lien, R.-C., Perlin, A., Nash, J. D., Gregg, M. C., & Wiles, P. J. (2009). Sea surface cooling at the Equator by subsurface mixing in tropical instability waves. *Nature Geoscience*, *2*(11), 761–765. https://doi.org/10.1038/ngeo657

Moum, J. N., Perlin, A., Nash, J. D., & McPhaden, M. J. (2013). Seasonal sea surface cooling in the equatorial Pacific cold tongue controlled by ocean mixing. *Nature*, *500*(7460), 64–67. https://doi.org/10.1038/nature12363

Murtugudde, R., Beauchamp, J., McClain, C. R., Lewis, M., & Busalacchi, A. J. (2002). Effects of penetrative radiation on the upper tropical ocean circulation. *Journal of Climate*, *15*(5), 470–486. https://doi.org/10.1175/1520-0442(2002)015<0470:EOPROT>2.0.CO;2

Ogata, T., Xie, S.-P., Wittenberg, A., & Sun, D.-Z. (2013). Interdecadal amplitude modulation of El Niño–Southern Oscillation and its impact on tropical Pacific decadal variability. *Journal of Climate*, *26*(18), 7280–7297. https://doi.org/10.1175/JCLI-D-12-00415.1

Philander, S. G. H. (1983). El Niño Southern Oscillation phenomena. *Nature*, *302*(5906), 295–301. https://doi.org/10.1038/302295a0

Reichl, B. G., Wittenberg, A. T., Griffies, S. M., & Adcroft, A. (2024). Improving equatorial upper ocean vertical mixing in the NOAA/GFDL OM4 model. *Earth and Space Science*, *11*(10), e2023EA003485. https://doi.org/10.1029/2023EA003485

Samanta, D., Karnauskas, K. B., & Goodkin, N. F. (2019). Tropical Pacific SST and ITCZ biases in climate models: Double trouble for future rainfall projections? *Geophysical Research Letters*, *46*(4), 2242–2252. https://doi.org/10.1029/2018gl081363

Schott, F. A., Mccreary, J. P., Jr., & Johnson, G. C. (2004). Shallow overturning circulations of the tropical-subtropical oceans. In *Earth's climate* (pp. 261–304). American Geophysical Union (AGU). https://doi.org/10.1029/147GM15

Sun, D.-Z., Yu, Y., & Zhang, T. (2009). Tropical water vapor and cloud feedbacks in climate models: A further assessment using coupled simulations. *Journal of Climate*, *22*(5), 1287–1304. https://doi.org/10.1175/2008jcli2267.1

Sverdrup, H. U. (1947). Wind-driven currents in a baroclinic ocean; with application to the equatorial currents of the eastern Pacific. *Proceedings of the National Academy of Sciences*, *33*(11), 318–326. https://doi.org/10.1073/pnas.33.11.318

Tang, T., Qi, L., Tozuka, T., Luo, J.-J., Ling, F., Luo, L., & He, J.-H. (2024). Emergent constraint on the projected central equatorial Pacific warming and northwestern Pacific monsoon trough change. *Environmental Research Letters*, *19*(5), 054003. https://doi.org/10.1088/1748-9326/ad3a80

Taylor, K. E., Stouffer, R. J., & Meehl, G. A. (2012). An overview of CMIP5 and the experiment design. *Bulletin of the American Meteorological Society*, *93*(4), 485–498. https://doi.org/10.1175/BAMS-D-11-00094.1

The NCAR Command Language. (2019). The NCAR Command Language (Version 6.6.2) [Software]. *UCAR/NCAR/CISL/TDD*. https://doi.org/10.5065/D6WD3XH5

Vannière, B., Guilyardi, E., Madec, G., Doblas-Reyes, F. J., & Woolnough, S. (2013). Using seasonal hindcasts to understand the origin of the equatorial cold tongue bias in CGCMs and its impact on ENSO. *Climate Dynamics*, *40*(3–4), 963–981. https://doi.org/10.1007/s00382-012-1429-6

Vialard, J., Jin, F.-F., McPhaden, M. J., Fedorov, A., Cai, W., An, S.-I., et al. (2025). The El Niño Southern Oscillation (ENSO) recharge oscillator conceptual model: Achievements and future prospects. *Reviews of Geophysics*, *63*(1), e2024RG000843. https://doi.org/10.1029/2024RG000843

Wallace, J. M., Rasmusson, E. M., Mitchell, T. P., Kousky, V. E., Sarachik, E. S., & von Storch, H. (1998). On the structure and evolution of ENSO related climate variability in the tropical Pacific: Lessons from TOGA. *Journal of Geophysical Research*, *103*(C7), 14241–14259. https://doi.org/10.1029/97JC02905

Wang, B., & An, S. I. (2002). A mechanism for decadal changes of ENSO behavior: Roles of background wind changes. *Climate Dynamics*, *18*(6), 475–486. https://doi.org/10.1007/s00382-001-0189-5

Wang, C., Zhang, L., Lee, S.-K., Wu, L., & Mechoso, C. R. (2014). A global perspective on CMIP5 climate model biases. *Nature Climate Change*, *4*(3), 201–205. https://doi.org/10.1038/nclimate2118

Whitt, D. B., Cherian, D. A., Holmes, R. M., Bachman, S. D., Lien, R.-C., Large, W. G., & Moum, J. N. (2022). Simulation and scaling of the turbulent vertical heat transport and deep-cycle turbulence across the equatorial Pacific cold tongue. *Journal of Physical Oceanography*, *52*(5), 981–1014. https://doi.org/10.1175/JPO-D-21-0153.1

Wilson, S. G. (2000). How ocean vertical mixing and accumulation of warm surface water influence the "sharpness" of the equatorial thermocline. *Journal of Climate*, *13*(20), 3638–3656. https://doi.org/10.1175/1520-0442(2000)013<3638:HOVMAA>2.0.CO;2

Wittenberg, A. T., Rosati, A., Lau, N. C., & Ploshay, J. J. (2006). GFDL's CM2 Global coupled climate models. Part III: Tropical Pacific climate and ENSO. *Journal of Climate*, *19*(5), 698–722. https://doi.org/10.1175/JCLI3631.1

Wittenberg, A. T., Vecchi, G. A., Delworth, T. L., Rosati, A., Anderson, W. G., Cooke, W. F., et al. (2018). Improved simulations of tropical Pacific annual-mean climate in the GFDL FLOR and HiFLOR coupled GCMs. *Journal of Advances in Modeling Earth Systems*, *10*(12), 3176–3220. https://doi.org/10.1029/2018MS001372

19448007, 2026, 7, Downloaded from https://agupubs.onlinelibrary.wiley.com/doi/10.1029/2026GL122108 by CochraneChina, Wiley Online Library on [08/11/2026]. See the Terms and Conditions (https://onlinelibrary.wiley.com/terms-and-conditions) on Wiley Online Library for rules of use; OA articles are governed by the applicable Creative Commons License

Wyrtki, K. (1981). An estimate of equatorial upwelling in the Pacific. *Journal of Physical Oceanography*, *11*(9), 1205–1214. https://doi.org/10.1175/1520-0485(1981)011<1205:aeoeui>2.0.co;2

Yeh, S.-W., Kug, J.-S., Dewitte, B., Kwon, M.-H., Kirtman, B. P., & Jin, F.-F. (2009). El Niño in a changing climate. *Nature*, *461*(7263), 511–514. https://doi.org/10.1038/nature08316

Ying, J., Huang, P., Lian, T., & Tan, H. (2019). Understanding the effect of an excessive cold tongue bias on projecting the tropical Pacific SST warming pattern in CMIP5 models. *Climate Dynamics*, *52*(3), 1805–1818. https://doi.org/10.1007/s00382-018-4219-y

Yuan, X., Jin, F.-F., & Zhang, W. (2020). A concise and effective expression relating subsurface temperature to the thermocline in the equatorial Pacific. *Geophysical Research Letters*, *47*(15), e2020GL087848. https://doi.org/10.1029/2020GL087848

Zebiak, S. E., & Cane, M. A. (1987). A model El Niño–southern oscillation. *Monthly Weather Review*, *115*(10), 2262–2278. https://doi.org/10.1175/1520-0493(1987)1152.0.CO;2

Zhang, Q., Zhu, Y., & Zhang, R.-H. (2023). Subsurface thermohaline biases in the Southern Tropical Pacific and the roles of wind stress and precipitation. *Journal of Climate*, *36*(7), 2293–2309. https://doi.org/10.1175/JCLI-D-22-0524.1

Zhang, W., Jin, F.-F., Stuecker, M. F., Wittenberg, A. T., Timmermann, A., Ren, H.-L., et al. (2016). Unraveling El Niño's impact on the East Asian Monsoon and Yangtze River summer flooding. *Geophysical Research Letters*, *43*(21), 11375–11382. https://doi.org/10.1002/2016gl071190

Zheng, Y., Lin, J.-L., & Shinoda, T. (2012). The equatorial Pacific cold tongue simulated by IPCC AR4 coupled GCMs: Upper ocean heat budget and feedback analysis. *Journal of Geophysical Research*, *117*(C5), C05024. https://doi.org/10.1029/2011jc007746

Zhou, Z. Q., & Xie, S. P. (2015). Effects of climatological model biases on the projection of tropical climate change. *Journal of Climate*, *28*(24), 9909–9917. https://doi.org/10.1175/jcli-d-15-0243.1

19448007, 2026, 7, Downloaded from https://agupubs.onlinelibrary.wiley.com/doi/10.1029/2026GL122108 by CochraneChina, Wiley Online Library on [08/11/2026]. See the Terms and Conditions (https://onlinelibrary.wiley.com/terms-and-conditions) on Wiley Online Library for rules of use; OA articles are governed by the applicable Creative Commons License